Experiments and modeling of bubble column dehumidifier performance

Emily W. Tow, John H. Lienhard V

Rohsenow Kendall Heat Transfer Laboratory
Department of Mechanical Engineering
Massachusetts Institute of Technology
Cambridge, Massachusetts 02139

Abstract

Humidification-dehumidification is a promising technology for decentralized, small-scale desalination, but conventional dehumidifiers are expensive due to the large surface area required. Direct-contact dehumidification in bubble columns has been shown to significantly decrease dehumidifier size and cost. In this paper, the heat flux and parallel-flow effectiveness of a bubble column dehumidifier are investigated experimentally using significantly smaller cooling coils than in previous work. In addition, a model is developed which predicts the heat transfer rate with an average error of less than 3%. It is found that heat flux rises and effectiveness decreases with decreasing coil area. Increasing air flow rate and air temperature both lead to increased heat flux but decreased effectiveness. Neither bubble-on-coil impact nor column height are found to significantly affect heat flux or effectiveness. The conflicting findings of previous research on bubble-on-coil impact are explained by the other trends identified in this work. Modeling results for salt water

*Address all correspondence to *lienhard@mit.edu*

April 24, 2014

temperature and tube diameter are presented. Additional heat transfer in the air gap above the column liquid is explored, but found to be minimal for well-designed columns with low temperature pinch. These findings will inform the design of bubble column dehumidifiers for high heat recovery and low capital cost.
Keywords: condensation, direct contact heat transfer, HDH desalination

---

Nomenclature

A	Coil immersed outer area [m^2]
D	Diameter [m]
M	Molar mass [kg/kmol]
N	Number [-]
P	Pressure [Pa]
R	Thermal resistance [K/W]
T	Temperature [°C]
Z	Thickness ratio, defined by Equation 14 [-]
$\dot{Q}$	Heat transfer rate [W]
$\dot{m}$	Mass flow rate [kg/s]
$\dot{q}$	Heat flux [W/m^2]
c_p	Specific heat at constant pressure [J/kg-K]

g Gravitational acceleration [m/s^2]

h Specific enthalpy [J/kg]

h_t Heat transfer coefficient [W/m^{2}K]

h_{fg} Latent heat of vaporization [J/kg]

k Thermal conductivity [W/m^2-K]

m Water vapor mass fraction [-]

u Velocity [m/s]

v_g Superficial gas velocity [m/s]

x Water vapor mole fraction [-]

Named Ratios

K Dean number, defined by Equation 13 [-]

Fr Froude number = u^2/gD [-]

Nu_D Nusselt number = $h_t D/k$ [-]

Pr Prandtl number = $\mu c_p/k$ [-]

Re Reynolds number = $\rho u D/\mu$ [-]

St Stanton number = $h_t/\rho c_p u$ [-]

Greek

ϵ Effectiveness [-]

μ Dynamic viscosity [Pa-s]

ν Kinematic viscosity [m^2/s]

ρ Density [kg/m^3]

σ Surface tension [N/m]

Subscripts

$//$ Parallel-flow

A Moist air stream

atm Atmospheric

B Bubble inner surface

b Bubble

C Column fluid

$cond$ Condensation

D Coil

da Dry air

E Coolant

f Liquid water

g Water vapor

h Sparger orifice

i In

ma Moist air

max Maximum

$meas$ Measured

o Out

sat Saturation

$turn$ Coil turn

w Water vapor

1. Introduction

Humidification-dehumidification (HDH) is a promising method for decentralized, small-scale desalination because of its simple system design and compatibility with low-grade energy [1] and a wide range of water compositions. In its most basic form, a HDH system consists of a heater, a humidifier, a dehumidifier, and the pumps and piping necessary to move fluid between components. Dehumidification technology warrants further study because of the high condenser area required [2, 3] to overcome the resistance to diffusion of a dilute vapor through air, and because the effectiveness of the dehumidifier dominates the performance of the entire HDH system [4].

Dehumidification in bubble columns has previously been shown to reduce device volume and condenser area by an order of magnitude [5]. A schematic diagram of the bubble column dehumidifier used in this work is shown in

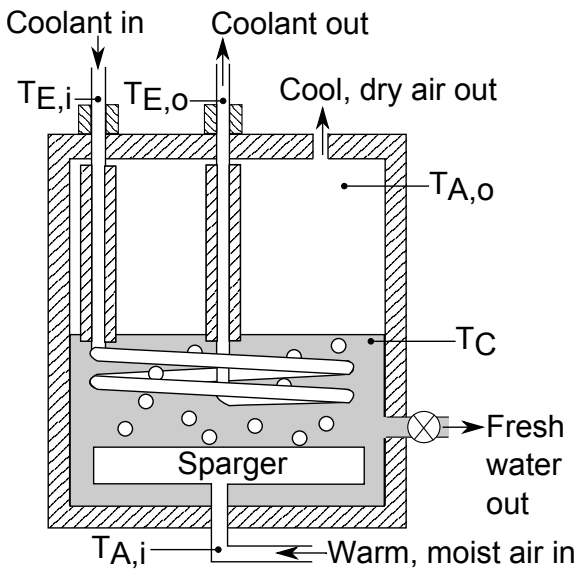

Figure 1: Schematic diagram of the experimental dehumidifier

Figure 1. In a bubble column dehumidifier, warm, moist air is bubbled though a column of fresh water cooled by indirect heat exchange with salt water. The concentration gradient from the warm bubble center to the cool bubble surface drives condensation on the surface of the bubble. The presence of non-condensable gas leads to a low condensation heat transfer coefficient. However, the key advantage of the bubble column dehumidifier lies in moving the condensation process off an expensive solid surface and onto the surface of a swarm of bubbles. The large interfacial area leads to very low resistance, and the heat leaving the bubbles is transferred to the cooling saline water at a high heat transfer coefficient through a coil with a small surface area.

In HDH desalination, bubble column dehumidifiers recover heat by using the saline feed water as a coolant in the dehumidifier, thereby preheating it for use in the humidifier. Multistage bubble columns further enhance this energy

recovery by minimizing the stage to stage temperature drop and allowing for thermal balancing (see [6, 7, 8]). In this paper, the thermal performance of a single stage bubble column dehumidifier is investigated experimentally using significantly smaller cooling coils than in previous work, and a predictive model is developed which shows very good agreement with the experimental data. The model presented here can be used to predict the performance of a multi-stage dehumidifier by modeling the performance of each stage.

Sieve tray columns, like multi-stage bubble columns with liquid in cross-flow, are commonly used in distillation and other vapor-liquid reactions. Barrett and Dunn [9] proposed a model for a sieve tray column dehumidifier or humidifier. In their dehumidifier, cold water enters in the top tray and warm, moist air is bubbled in from the bottom. Given a source of cold water, such a dehumidifier would require no cooling coils and could be quite inexpensive. However, the cold water source in HDH is saline water, and dehumidifying moist air from the humidifier by direct contact with saline water in a tray column would not result in the production of any fresh water. Because the cooling saline water and condensing fresh water must be kept separate, the dehumidifier used in the present experimental investigation contains the saline water within a copper coil, necessitating a new heat transfer model.

The heat and mass transfer processes in bubble column dehumidifiers are not yet well characterized. Bubble column reactors have been studied extensively as gas-liquid reactors where the mass diffusion resistance between the bubble surface and the bulk liquid dominates the performance of the column [10]. Additionally, practical bubble column dehumidifiers for HDH desalination need to be very short to ensure a minimal gas-side pressure drop,

and several researchers have noted that the gas and liquid phases behave differently near the gas inlet [10, 11, 12, 13]. Most bubble column reactors are significantly taller than those used for dehumidification [5, 10], so the entry region is often neglected in the reactor modeling and design literature. A model by Narayan et al. [5] proposes a thermal resistance network for the bubble column dehumidifier with transport mechanisms taken from the bubble column reactor literature. This model predicts the heat flux with moderate accuracy in simple configurations, but it calls for refinement. Another model [14] proposes a different resistance network along with mean heat and mass transfer driving forces in the bubble stream, but does not predict heat and mass transfer coefficients. The model presented in this paper addresses many of these outstanding issues.

Because the cost of a bubble column dehumidifier is strongly influenced by the mass of copper used in the coil, the experiment performed in this work uses much shorter cooling coils than those used by Narayan et al. [5] with the aim of achieving higher a heat flux on the coil surface. However, changes to the column design (e.g., coil length) or operation (e.g., air temperature) that increase the heat flux may reduce capital cost, but may also reduce the effectiveness of the dehumidifier. By measuring the parallel-flow effectiveness, the effect of changes to the column design and operation can be quantified in terms of heat flux and effectiveness to give insight into both capital and energy costs.

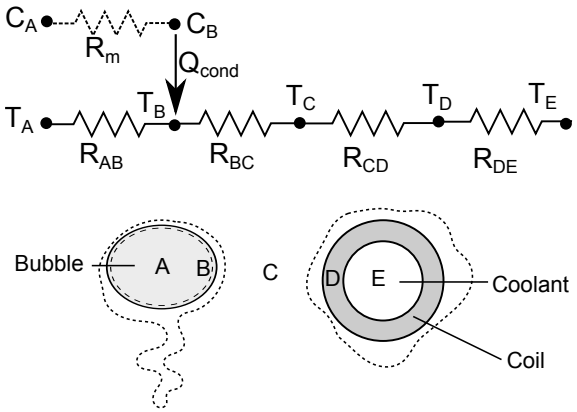

Figure 2: Resistance network from [14] governing heat and mass transfer in a bubble column

2. Theory

Heat and mass transfer in the single-stage bubble column dehumidifier can be described by the resistance network in Figure 2. The system is modeled as suggested in [14] with one critical modification: the gas-side heat and mass transfer resistances (the left side of Figure 2) are considered to be negligible. The dehumidifier is modeled as a single-stream heat exchanger with the well-mixed column liquid as the isothermal stream.

Given the assertion by previous authors [5] that the gas-side resistance has a significant effect on bubble column dehumidifier performance, the presently applied approximation of negligible gas-side resistance clearly merits justification. In this section, a brief review of bubble size correlations is performed and the evidence in support of neglecting the gas-side resistances is presented. A model is then detailed which predicts heat transfer rate and heat flux in the dehumidifier. Finally, the parallel-flow effectiveness [15], a performance pa-

rameter relevant to individual well-mixed bubble column dehumidifier stages, is defined.

2.1. Bubble-Side Resistance

Limited attention has been devoted to the prediction of heat transfer coefficients inside and outside the bubbles because mass transfer resistance dominates in most industrial bubble column reactor applications. Because liquid-phase mass transfer in bubble columns is well-studied, an analogy to mass transfer could easily be used to approximate the thermal resistance between the bubble surface and the bulk column liquid (R_{BC} in Figure 2). However, the heat and mass transfer resistances inside the bubble (R_{AB} and R_m in Figure 2, respectively) are elusive.

Narayan et al. [5] propose a model for bubble column dehumidifier performance which treats the heat and mass transfer inside the bubbles. However, the model relies on several unconfirmed assumptions. The authors give a conservative estimate of the heat transfer coefficient using a Lewis factor [16, 17] mass transfer analogy, with mass transfer inside the bubble approximated as steady diffusion through a slab with thickness equal to the bubble radius. This leads to the prediction that heat flux can be improved by reducing the bubble diameter and that hitting the cooling coils can improve heat transfer. Finally, they also predict a non-zero mass transfer resistance to the unphysical [9] diffusion of the condensed liquid water through the identical column liquid water.

Daous and Al-Zahrani [18] measure the heat and mass transfer resistances experimentally, but the resulting heat transfer coefficient is surprisingly low. They find that in the homogeneous flow regime ($v_g < 5$ cm/s [10]), the prod-

uct of the heat transfer coefficient and specific interfacial area is between 1 and 20 W/m^3-K. Considering that the specific interfacial area in homogeneous flow is on the order of 100 m^{-1} [19], the measured heat transfer coefficients would have to be around 0.01 to 0.2 W/m^2-K, far lower than the equivalent heat transfer coefficient for conduction through a stagnant air sphere (order 10 W/m^2-K) of a typical bubble size. In contrast, it would be expected that bubble oscillations, inner circulation, and breakup and coalescence would raise the heat transfer coefficient well above the conduction-only equivalent.

However, several studies suggest that the bubble-side resistance to heat and mass transfer is negligible. A review by Kanatarci et al. [10], like much of the bubble column literature, discusses the liquid-to-wall heat transfer in detail while giving no mention of the mechanism of heat transfer (or mass transfer, for that matter) *through* the bubbles. In their model of a sieve-tray-column dehumidifier, Barrett and Dunn assume that "both gas and liquid phases are...perfectly mixed so that the conditions of the gas and liquid streams leaving a tray are representative of conditions on the tray" [9]. Perfect mixing implies that the bubbles take on the temperature of the surrounding liquid, or that the resistance is essentially zero. Kang et al. [20] use a non-zero internal heat transfer coefficient proposed by Clift et al. [21] in their comparison of bubbling and falling-film modes of ammonia-water absorption, but it is clear from their results that the overall resistance inside the bubbles is very low. When cold gas bubbles are introduced into a vertical channel with hot walls, their simulation shows that the bubble temperature rises rapidly, becoming almost indistinguishable from the wall temperature

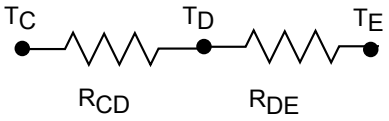

Figure 3: Simplified thermal resistance network

within the first 4-5 cm of rise. Considering that the need to immerse the coil mandates a minimum height of 4 cm in this work, the results of Kang et al. suggest that it is reasonable to neglect resistance in the gas phase in the present model. Finally, as explained in [14], if the gas side resistance R_{AB} can be neglected, so can the liquid-side resistance just outside the bubbles, R_{BC}, leading to the assumption of perfect mixing within the short column and enabling simple modeling of the bubble column dehumidifier.

2.2. Heat and Mass Transfer Model

The perfect mixing assumption justified in Section 2.1 greatly simplifies the transport modeling. The bubble column dehumidifier acts like a single-stream heat exchanger with the well-mixed column liquid as the isothermal stream. The temperature of the column liquid is dependent on the coil-side thermal resistance—the right half of Figure 2, or the entirety of the simplified resistance network, Figure 3—and the temperatures and flow rates of the moist air and coolant streams. The overall resistance through the coil can be estimated using correlations found in the literature. The set of equations that make up the proposed model are not linear, and an equation solver such as Engineering Equation Solver (EES) [22], used here with the built-in physical properties of air and water, is recommended.

Due to the small hydrostatic head of the short column, all properties are

evaluated at atmospheric pressure. All water is assumed to be pure, although in practice seawater would generally be used as a coolant (inside the tube) for a dehumidifier used in HDH desalination.

Assuming the column operates in steady state and is well insulated such that a negligible quantity of heat is lost to the environment, Equation 1 shows that the total heat transfer rate into the coolant, $\dot{Q}_{CE}$, is the sum of the sensible and latent heat transfer rates out of the bubbles, $\dot{Q}_{AB}$ and $\dot{Q}_{cond}$, respectively:

$$\dot{Q}_{CE} = \dot{Q}_{AB} + \dot{Q}_{cond} \tag{1}$$

In the present experiment, the air entering the column is assumed to enter saturated with water. The mass flow rate of dry air and the inlet water vapor mass flow rate are related to the inlet saturated mass fraction by Equations 2 and 3:

$$\dot{m}_{da} = \dot{m}_{ma,i}[1 - m_{sat,i}] \tag{2}$$

$$\dot{m}_{w,i} = \dot{m}_{ma,i} m_{sat,i} \tag{3}$$

The water vapor-air mixture is assumed to behave ideally. As explained in [14], Equation 4 represents the conservation of energy for the entire moist air stream. The air exit temperature must be equal to the column temperature to satisfy the approximation of zero gas-side resistance.

$$\begin{aligned} \dot{Q}_{AB} &= \dot{m}_{da}[h_{da}(T_{A,i}) - h_{da}(T_C)] \\ &+ \dot{m}_{w,i}[h_g(T_{A,i}) - h_g(T_C)] \end{aligned} \tag{4}$$

Equation 5 gives the latent heat released when water vapor condenses at the bubble surface:

$$\dot{Q}_{cond} = \dot{m}_{cond} h_{fg}(T_C) \tag{5}$$

Equation 6 relates the heat transfer to the coolant to its change in enthalpy.

$$\dot{Q}_{CE} = \dot{m}_E[h_E(T_{E,o}) - h_E(T_{E,i})] \tag{6}$$

Due to the near-unity Lewis factor of water vapor in air [16], it is expected that mass transfer rates will keep up with the heat transfer rates such that the air leaves in a saturated state at the column liquid temperature, T_C. Equation 7 gives the saturated air outlet mole fraction.

$$x_o = \frac{P_{sat}(T_C)}{P_{atm}} = \frac{\dot{m}_{w,o}/M_w}{\dot{m}_{w,o}/M_w + \dot{m}_{da}/M_{da}} \tag{7}$$

The condensation mass flow rate, $\dot{m}_{cond}$, is a parameter of great interest in water purification applications:

$$\dot{m}_{w,i} = \dot{m}_{w,o} + \dot{m}_{cond} \tag{8}$$

Next, the heat transfer driving force is discussed. Due to the excellent mixing in the bubble column, there is a negligible radial temperature gradient [23] and essentially zero resistance to radial mixing. Though temperature gradients have been observed in the vertical direction in industrial bubble columns [24], the depth of the liquid used in this experiment is only about 1-10% of the height of a typical bubble column. Therefore, the column liquid is expected to be isothermal except very close to the cooling coil. It is also assumed that due to the good wettability of the copper coil, the tube only directly contacts the column liquid and not the air bubbles. For these reasons, the log-mean temperature difference (LMTD) for a single-stream heat exchanger is used to model the thermal driving force across the coil:

$$\Delta T_{LM,CE} = \frac{T_{E,o} - T_{E,i}}{\ln\left(\frac{T_C - T_{E,i}}{T_C - T_{E,o}}\right)} \tag{9}$$

Equation 10 shows the relationship of the total heat transfer $\dot{Q}_{CE}$ to the LMTD and the total thermal resistance as shown in Figure 3:

$$\dot{Q}_{CE} = \frac{\Delta T_{LM,CE}}{R_{DE} + R_{CD}} \tag{10}$$

It is assumed that all heat transfer occurs within the liquid portion of the column. Heat transfer from the outgoing air to the exposed portion of the coil in the air gap (see Figure 1) is neglected because in practice, size and cost restrictions will enforce a short air gap and a small exposed area of coil. Thermal resistance through the tube wall is neglected because a thin copper tube is used in the experiment discussed herein, but a third resistance can easily be added in series to account for a more resistive tube material.

The convective resistances in Equation 10 are related to the relevant heat transfer coefficients and areas by Equation 11.

$$R_{CD} = \frac{1}{h_{t,CD} A_{D,o}} \quad \text{and} \quad R_{DE} = \frac{1}{h_{t,DE} A_{D,i}} \tag{11}$$

The heat transfer coefficients inside and outside the coils are relatively well-studied. Appropriate formulations were developed by Mori and Nakayama [25] for the heat transfer coefficient inside curved tubes of round cross-section in laminar flow. Secondary flows induced by the coil curvature significantly reduce the radial length scale for convection compared to a straight tube. For example, the curved pipe Nusselt number in this experiment is predicted to be nearly ten times the straight pipe value. This curvature-induced augmentation of the heat transfer coefficient extends, to a lesser extent, into turbulent flow [26]. Equation 12 gives the Nusselt number correlation for laminar flow in a curved tube based on the Dean number K and the thick-

ness parameter Z [25]:

$$\mathrm{Nu}_{D,DE} = \frac{h_{t,DE} D_{D,i}}{k_E} = 0.8636\left(\frac{K^{1/2}}{Z}\right) \tag{12}$$

Equation 13 gives the Dean number:

$$K = \mathrm{Re}_E \left(\frac{D_{D,i}}{D_{turn}}\right)^{1/2} \tag{13}$$

For Pr> 1 (e.g., for water), the thickness parameter Z is given by Equation 14:

$$Z = \frac{2}{11}\left(1 + \sqrt{1 + \frac{77}{4}\mathrm{Pr}_E^{-2}}\right) \tag{14}$$

Kantarci et al. [10] provide an excellent review of many bubble column design considerations including correlations for the heat transfer coefficient. Perhaps the most widely used correlation comes from Deckwer [27] for heat transfer to a large surface such as the column wall. Several correlations have been proposed for heat transfer to small cylindrical heat exchange surfaces [28, 29, 30, 31], but there is significant disagreement among them. Because the smaller length scale of internal heat transfer equipment is likely, if anything, to augment heat transfer, Deckwer's model for heat transfer to an infinitely-large surface is used here as a conservative estimate of the heat transfer coefficient.

Deckwer's model is based on the idea that the bubbles' flow work is dissipated by small eddies which interact periodically with the heat transfer surface. The interactions are modeled as conduction through a semi-infinite slab with a characteristic time equal to the ratio of the characteristic eddy length and characteristic velocity. An empirically-derived constant leads to a Stanton number correlation, Equation 15 [27]:

$$\mathrm{St} = 0.1(\mathrm{ReFrPr}^2)^{-1/4} \tag{15}$$

The present authors find the dimensionless form unsatisfactory because both Re and Fr involve an unspecified length dimension which cancels out when they are multiplied. The dimensional form is given by Equation 16:

$$h_{t,CD} = 0.1 k_f^{1/2} \rho_f^{3/4} c_{p,f}^{1/2} \mu_f^{-1/4} g^{1/4} v_g^{1/4} \tag{16}$$

Perhaps a more illustrative representation is given by Equation 17, an equivalent Nusselt number correlation based on Deckwer's characteristic eddy length η [27]:

$$\mathrm{Nu}_\eta = 0.1\mathrm{Pr}^{1/2} \tag{17}$$

where

$$\eta = \left(\frac{\nu^3}{v_g g}\right)^{1/4}. \tag{18}$$

The superficial velocity v_g in the above relationships is the ratio of gas volume flow rate to column cross-sectional area. In predicting the outcome of the present experimental results, the superficial velocity is calculated based on the sparger area because of the coil's close proximity to the sparger.

The equations in this section can be solved to find the total heat transfer, $\dot{Q}_{CE}$, and the heat flux through the coil, $\dot{q}$:

$$\dot{q} = \frac{\dot{Q}_{CE}}{A}, \tag{19}$$

where A is the outer surface area of tubing that is immersed in the column liquid.

2.3. Parallel-Flow Effectiveness

Tow and Lienhard [15] propose parallel-flow effectiveness as a new performance parameter for individual bubble column dehumidifier stages. In contrast to the effectiveness defined by Narayan et al. [32] for simultaneous heat and mass exchangers, by which bubble columns can be compared to other (generally counterflow) dehumidifier types, the parallel-flow effectiveness acknowledges that as long as the column fluid is well-mixed, each bubble column stage acts like a parallel-flow device.

Compared to counterflow dehumidifiers, the effectiveness of a well-mixed single-stage bubble column dehumidifier is low (around 50%) because of the interaction of both streams with the well-mixed column liquid. This leads to the need for multi-stage devices. Narayan and Lienhard [6] demonstrated that combining bubble column stages at different liquid temperatures into a multi-staged device with an overall counterflow configuration can achieve effectiveness comparable to conventional dehumidifiers.

However, effective multi-staging requires each stage of the column to have a low enthalpy pinch [33]. Enthalpy pinch represents an improvement over temperature pinch as a performance parameter for simultaneous heat and mass exchangers because of the nonlinearity of the enthalpy-temperature curve of saturated moist air, but it is still a dimensional quantity. Good heat recovery requires that each stage achieve a large fraction of its maximum single-stage heat transfer rate. Therefore, to compare the effects of various parameters on the heat recovery of a single column stage, a parallel-flow effectiveness, $\epsilon_{//}$, is defined in [15] by Equation 10:

$$\epsilon_{//} = \frac{\dot{Q}_{CE}}{\dot{Q}_{max,//}}, \tag{20}$$

where $\dot{Q}_{max,//}$ is the total heat transfer rate $\dot{Q}_{CE}$ from Section 2.2, except with *all* outlet temperatures equal to the column liquid temperature, or equivalently, with all resistances evaluated as zero.

Meaningful performance parameters give insight into the cost per unit of fresh water produced of operating the dehumidifier in a HDH system. The fresh water production is strongly linked to the heat transfer rate because the majority of the heat removed from the air stream is latent heat. The coil, generally copper, represents a capital expense, and the heat flux determines the coil area needed for a system of a particular capacity. The effectiveness, on the other hand, relates to the energy use and cost of HDH desalination using a bubble column dehumidifier. Effectiveness is a function of the number of stages (see [6]), the thermodynamic balancing (see [33]), and, finally, the parallel-flow effectiveness of each stage. Changes to the column design and operation will be analyzed in this work in terms of both heat flux and parallel-flow effectiveness to capture effects on both capital and energy costs.

Because only single-stage bubble columns are considered in this paper, all further references to effectiveness will denote the parallel-flow effectiveness, $\epsilon_{//}$. In tests where $\dot{Q}_{max,//}$ and coil area, A, are constant (e.g., while varying column liquid height), only effectiveness will be plotted because the heat flux is related to effectiveness by a constant as in Equation 21:

$$\dot{q} = \epsilon_{//}\left(\frac{\dot{Q}_{max,//}}{A}\right) \tag{21}$$

3. Experimental Methods

Heat flux and parallel-flow effectiveness are measured for a variety of conditions. Coil length, air temperature, column liquid height, and sparger orifice size are varied. Additionally, in order to make meaningful comparisons to previous studies, the effect of bubble-on-coil impact is isolated and reported. In total, 24 measurements (each in terms of heat flux and effectiveness) are made.

3.1. Experimental Bubble Column Dehumidifier

Dehumidifier heat flux and effectiveness are measured with an instrumented HDH system. The 28 cm square by 36 cm high dehumidifier can be filled to any desired height. The moist air temperature and the air and coolant flow rates are adjustable. The experimental dehumidifier is shown in Figure 4.

Moist air enters the dehumidifier from a humidifier, in which compressed dry air is forced through a porous stainless steel cartridge sparger into a tank heated by a submerged resistance heater. The moist air leaves the humidifier close to saturation, and it cools slightly as it passes through insulated rubber tubing and a rotameter to the dehumidifier. Condensation in the rotameter establishes that the air entering the dehumidifier is saturated.

The effect of condensation in the rotameter on the flow rate reading is neglected, but the difference in density of the warm, moist air from the dry air at STP for which the rotameter is calibrated is accounted for. Because gas flow in a rotameter is largely inviscid, the flow rate reading is proportional to the square root of the density, leading to Equation 22, the correction factor

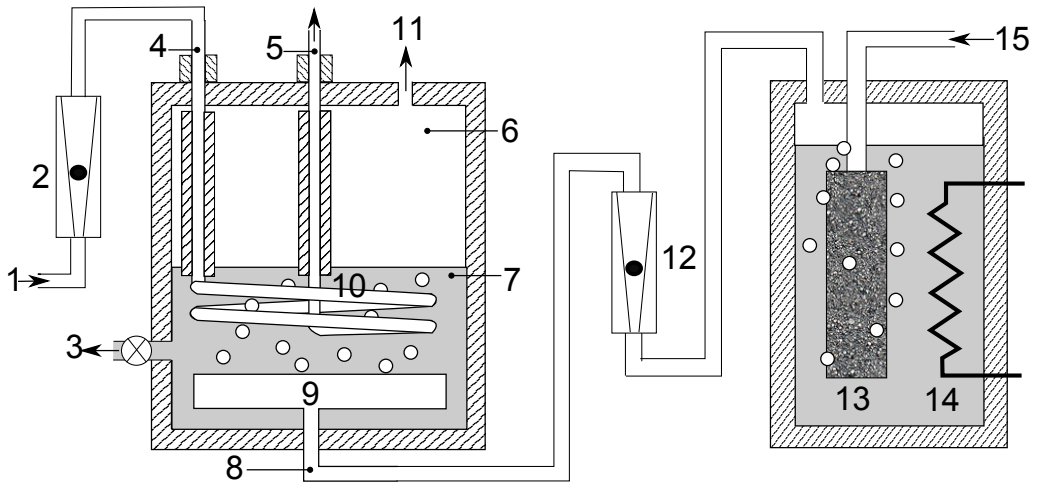

Figure 4: Experimental setup: (1) pressurized cooling water inlet, (2, 12) rotameters, (3) fresh water outlet valve, (4-8) thermocouples, (9) plate sparger, (10) cooling coil, (11) air outlet, (13) cartridge sparger. (14) resistance heater, (15) pressurized dry air inlet

from [15]:

$$\frac{\dot{V}_{ma}}{\dot{V}_{meas}} = \sqrt{\frac{\rho_{da,STP}}{\rho_{ma}(T_{A,i})}} \tag{22}$$

All cooling coils were made from 9.5 mm OD, 8.0 mm ID copper tubes. The two larger coils had an 8.5 cm turn radius. The medium-sized (67 cm) coil, which was used in the present work except where noted, was a single loop. An impractically small (8.7 cm long) "coil" was included to illustrate the trade-off between heat flux and effectiveness. For reference, the largest coil used here (900 cm^2) was comparable in length and equivalent in tube diameter to the coils used by Narayan et al. [3]. The vertical part of each coil, which connects the immersed portion to the chilled water source, was insulated by 3.2 mm thick, 9.5 mm ID rubber tubing.

The coolant used in the present experiment was tap water, but it will be referred to as "coolant" in this paper to provide distinction from the liquid (also tap water) in the column. The coolant flow rate in all trials was 0.5 L/min, corresponding to laminar flow at a Reynolds number of 1740.

Equation 6 was used to find the heat transfer rate from the coolant stream. Equations 1, 2, 4, 5, 7, and 8 were used with the temperature and air flow rate measurements, assuming 100% relative humidity of all air streams, to calculate the heat transfer rate to the air stream. In steady state and with no heat exchange with the environment, the heat transfer rates from the coolant and to the air stream should be equal. In practice, however, it was difficult to maintain all streams and the column at constant temperature and flow rate, and the heat transfer rate was calculated from the average of the two measurements. There is some measurement uncertainty, primarily due to the 1.1 K uncertainty of the K-type thermocouples and the 5-10% uncertainty associated with the rotameter readings. The averaging of air-side and coolant-side heat transfer rate measurements reduces the overall uncertainty, leading to a 95% confidence interval of $\pm$29 W (10-15%) around each heat transfer rate measurement.

3.2. Controlling Bubble-on-Coil Impact

Bubble-on-coil impact is a design parameter proposed by Narayan et al. [5]. Releasing bubbles such that they will hit the cooling coil has several potential benefits. As suggested by Narayan et al. [5], the gas bubbles might directly contact the cooling coil, introducing a conduction path unmediated by the column liquid. Bubbles hitting the coil could also change shape, affecting the boundary layer thickness both inside the bubble and out, or split or

slow down, increasing the total interfacial area. Bubbles rising in the vicinity of the coil may alter the thermal resistance outside the coil by changing the bulk velocity or by periodically thinning the coil's boundary layer. These and other possible phenomena are difficult to isolate. However, by using different coils for the "impact" and "non-impact" cases, Narayan et al. [5] neglected to control two additional parameters, one of which significantly affects the heat flux. First, coil surface area is shown in Section 4.2 to have a very strong influence on heat flux, especially for long coils with high effectiveness. Therefore, coil surface area should be kept constant when another parameter is being evaluated. In addition, coil shape affects the heat transfer coefficient inside the coil due to the secondary flows that form in curved pipes, which have a more pronounced effect in coils of smaller turn radius [25], and the high heat transfer coefficients in the thermal entry region after a sharp bend.

In order to test the effect of bubble-on-coil impact without changing the coil shape or size, the pattern of sparger holes was modified—without altering the size or number of holes—to inject streams of bubbles that would or would not hit the coil. Duct tape, which sticks well to the acrylic sparger plate when wet, was used to cover unused holes as shown in Figure 5. The column was examined visually during operation to confirm that bubbles were hitting the coil in the impact case. Varying bubble-on-coil impact by changing only the pattern of sparger holes allows the effect of bubbles hitting the coils to be distinguished from the effects of changes to the coil design.

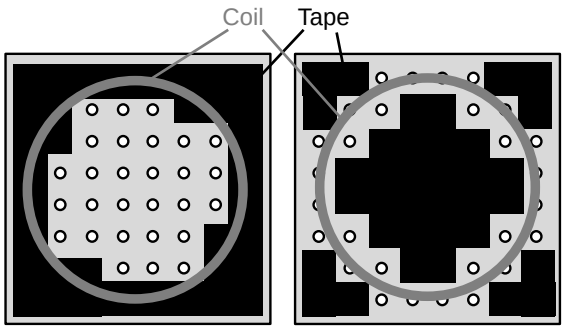

Figure 5: The sparger orifice configurations used to test the effect of bubble-on-coil impact without altering the coil for the small (2.8 mm) orifices

4. Results

In this section, agreement is demonstrated between experimental results and the proposed model. The effects of variations in coil surface area, air inlet temperature, and column liquid height on heat flux and parallel-flow effectiveness are shown. The additional heat transfer that occurs in the air gap above the column liquid is discussed, and finally, predictions are made regarding the effect of coolant temperature and tube diameter on performance.

4.1. Model Agreement

The model developed herein displays very good agreement with the experimental data both from this work and from [15] for a well-mixed, coil-cooled, single-stage bubble column dehumidifier. Figures 6 and 7 show the agreement in terms of heat transfer rate and effectiveness, respectively. In no case does the model accurately predict the performance of the extremely short (8.7 cm long) coil, shown in grey. The low effectiveness of the short coil forces a significant amount of heat transfer to occur in the air gap, as will be discussed

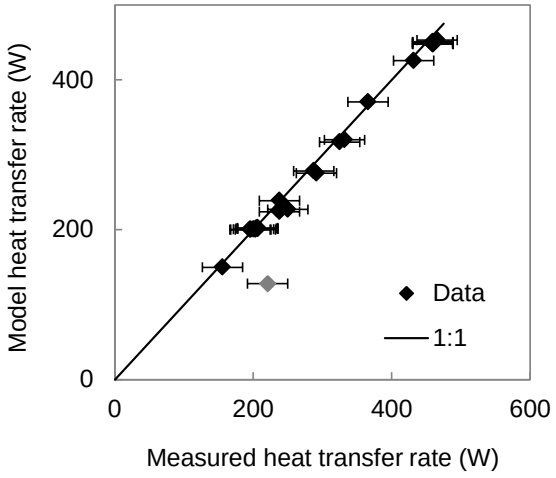

Figure 6: Agreement between theoretical predictions of heat transfer rate and all 24 experimental measurements

in Section 4.5. In addition, the measured heat transfer rate leaving the air stream was 64% higher than that entering the coolant stream, which suggests that leakage of coolant during this measurement was likely. However, this measurement was included in the experimental results for completeness. However, all other data is in excellent agreement with an average absolute error of 2.8%.

4.2. Coil Length

The relationship between coil length and parallel-flow effectiveness is clear, but even more marked is the effect of coil length on heat flux. Figures 8 and 9 show these trends for coils of constant tube diameter using experimental data from [15] at constant air and coolant temperatures and flow rates. Effectiveness increases with coil length, asymptotically approaching a value of one when the coil gets very long. Clearly, the longest (3 m) coil is "very

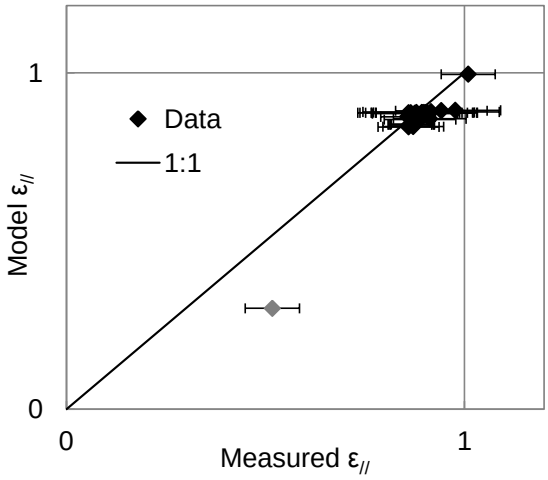

Figure 7: Agreement between theoretical and experimental parallel-flow effectiveness. It is clear from the cluster around $\epsilon_{//} = 0.85$, corresponding to the 67 cm coil, that the coil size all but determines the effectiveness.

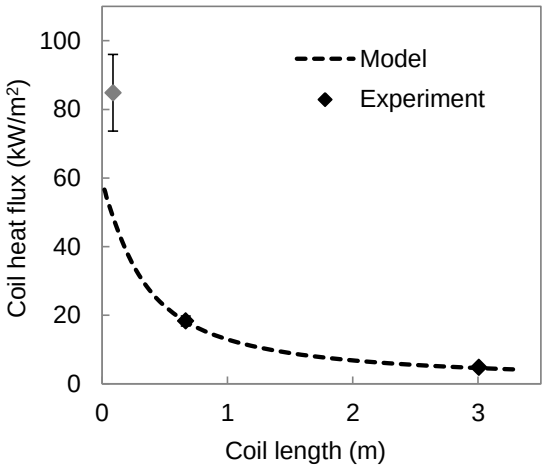

Figure 8: The effect of coil length on heat flux

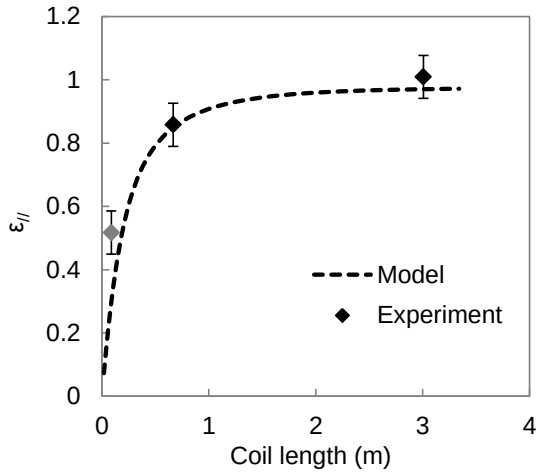

Figure 9: The effect of coil length on effectiveness

long" for this device. Although a value of one is within the margin of error for the parallel-flow effectiveness of this coil, the *parallel-flow* effectiveness *can exceed* unity due to thermal interaction between the air and coolant streams in the air gap above the column liquid. This phenomenon is neglected in the definition of $\epsilon_{//}$ but is discussed in Section 4.5. The effect of coil length on effectiveness is not pronounced except at very small lengths because the heat transfer rate is not strongly dependent on coil length and the maximum single-stage heat transfer rate is independent of coil size. Therefore, heat flux—the heat transfer rate per unit coil area—rises sharply as the coil size is reduced. Because the heat flux gained by minimizing the coil area is accompanied by a loss of effectiveness, the optimal coil size must be determined by analyzing the cost and performance of a complete HDH system.

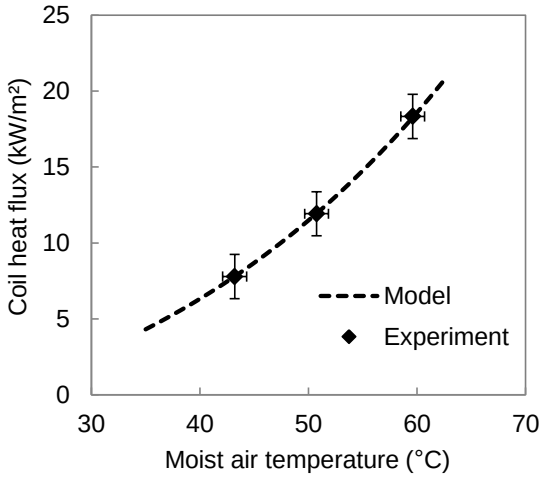

Figure 10: The effect of moist air inlet temperature on heat flux

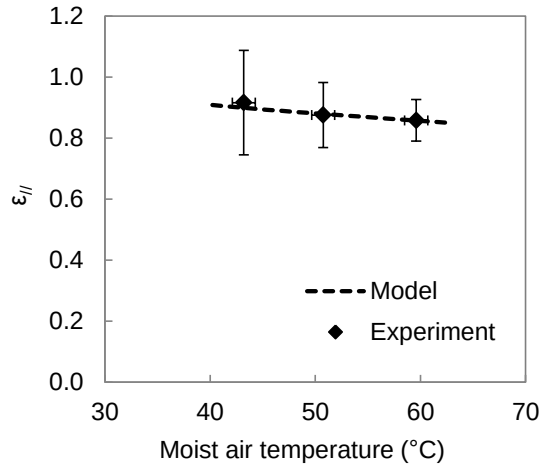

Figure 11: The effect of moist air inlet temperature on effectiveness

4.3. Moist Air Temperature

The effects of varying moist air inlet temperature on heat flux and effectiveness are shown in Figures 10 and 11 using experimental data from [15], with which the model is in excellent agreement. Heat flux increases sharply with moist air temperature because both the higher temperature and the higher concentration of condensible water vapor contribute to the enthalpy of the warmer moist air. However, effectiveness decreases with increasing air temperature because the heat transfer coefficients of the coil are near-constant, forcing the much greater heat flux to occur over greater mean temperature differences, thus widening the temperature pinch and decreasing the effectiveness.

4.4. Liquid Height, Sparger Orifice Size, and Bubble-on-Coil Impact

Column liquid height, sparger orifice size and bubble-on-coil impact are discussed together in this section because of their possible effects on the gas side of the extended resistance network, Figure 2, which was neglected in the present model.

Narayan et al. [5] found that heat flux was independent of liquid height for heights above 15 cm, the minimum height necessary to cover their large cooling coil. However, they hypothesize that the critical height, above which heat flux is independent of liquid height, is on the order of the bubble diameter [5]. The 67 cm coil used here had only one loop, and therefore the minimum height that could be tested was lower than the minimum tested in [5], about 4 cm. Liquid height was measured at the side of the column during bubbling. Though the model presented here includes no dependence on column height, experiments were conducted at different column heights

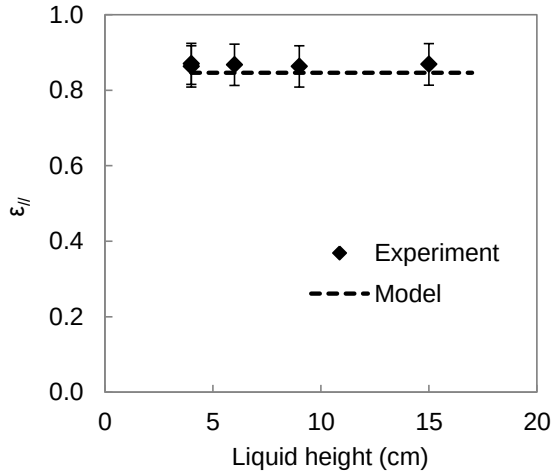

Figure 12: For 2.8 mm orifices and liquid height above 4 cm, effectiveness is independent of liquid height

to justify the assumption that bubble-side resistance is negligible. Figure 12 compares the height-independent model to experimental data from [15]. Figure 12 shows that for homogeneous flow through the 2.83 mm orifice plate, any critical height must be below 4 cm. The air temperature and flow rate were 58.4°C and 2.1 L/s and the coolant temperature was 16.6 ± 0.3 °C. The heat flux, not shown, was just over 23 kW/m^2 for all heights.

The absence of any decrease in effectiveness at heights as low as 4 cm suggests that much of the heat transfer occurs early in each bubble's residence in the column. Although it is difficult to verify the claim of Narayan et al. [5] that the critical height is on the order of the bubble diameter (a few millimeters) these results are consistent with that hypothesis. Minimizing the liquid height will improve bubble column performance by reducing the hydrostatic contribution to the air inlet pressure, thereby reducing the

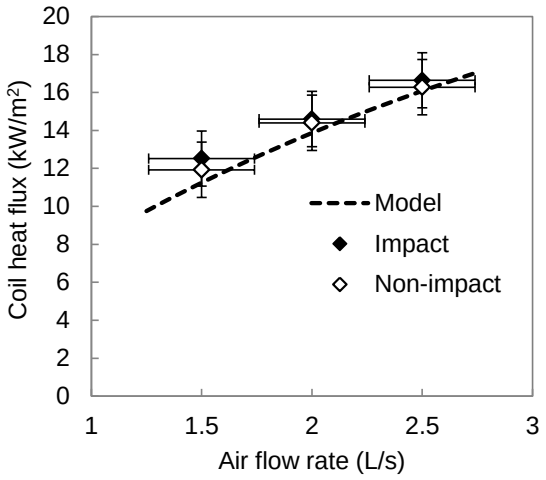

Figure 13: For 2.8 mm orifices and small bubbles, the effect of bubble-on-coil impact on heat flux is small

power needed to pump the air. Fortunately a depth of 4 cm corresponds to a hydrostatic pressure drop of only about 400 Pa per stage, or 2 kPa for a five-stage dehumidifier. Using narrower tubes so that the liquid height which just covers the coil can be reduced further lowers the pressure drop, as shown by Narayan et al. [34] who demonstrate a three-stage bubble column dehumidifier with an 800 Pa pressure drop.

Using the same sparger with small (2.83 mm) orifices, Figures 13 and 14 demonstrate the effect of bubble-on-coil impact for three air flow rates. As discussed in Section 3.2, bubble-on-coil impact was varied by changing the pattern of sparger orifices rather than changing the coil. The air temperature was 48.8 ± 0.4 °C and the coolant temperature was 15.8 ± 0.6 °C. The column height was 20 cm.

The effect of bubble-on-coil impact in Figures 13 and 14 was within the

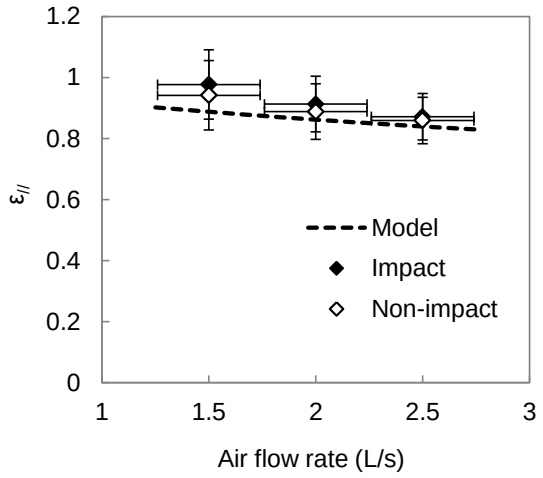

Figure 14: For 2.8 mm orifices and small bubbles, the effect of bubble-on-coil impact on effectiveness is small

margin of error of the experiment for all three air flow rates. This is not surprising given the observation of Narayan et al. [5] that increasing the liquid height beyond what is required to cover the cooling coil, which would have the effect of decreasing the gas-side resistance, does not increase the heat flux. The observation that neither liquid height nor bubble-on-coil impact can significantly change the effectiveness serves to justify the assumption of negligible gas-side resistance. Small changes in effectiveness with bubble-on-coil impact may be due to variation in the outside-coil heat transfer coefficient.

This finding that bubble-on-coil impact does not significantly raise the heat flux or effectiveness is in conflict with the observation by Narayan et al. that bubble-on-coil impact "raises the heat transfer rates to significantly higher values" [5]. Their claim is supported by a chart which shows that heat *flux* (in units of kW/m^2) is about twice as high with bubble-on-coil impact

as without [5]. Neither coil surface area nor inlet air temperature is specified, though both parameters have been shown in the present work to have strong effects on heat flux. Thus, it is not impossible that the use of different coil areas and/or air temperatures led Narayan et al. [5] to obtain very different heat flux measurements without any significant heat transfer augmentation from bubble-on-coil impact.

Because all runs in Figure 6 have high effectiveness, it could be argued that bubble-on-coil impact would have a more significant effect at lower effectiveness. However, given that bubble impact had no meaningful effect at the lowest effectiveness in Figure 14 (87%), a significant difference such as that reported by Narayan et al. [5] would be unlikely to occur due to bubble-on-coil impact alone in a column designed for high effectiveness.

Regardless of bubble impact, Figures 13 and 14 show that heat flux increases and effectiveness decreases with increasing air flow rate. The increase in heat flux is due to the increase in maximum single-stage heat transfer rate. The decrease in effectiveness occurs because the thermal driving force and resistance across the coil are largely unchanged while the maximum heat transfer rate increases.

Larger, 6.0 mm sparger orifices were tested with the aim of producing larger bubbles [13] whose gas-side resistance might be greater and also more significantly affected by changes to the column liquid height and bubble-on-coil impact. The effect of height and impact for the large orifices is shown in Figure 15. The air temperature and flow rate were 47.8 °C and 1.5 L/s and the coolant temperature was 20.2 ± 0.2 °C.

For the 6.0 mm sparger orifices, bubble-on-coil impact has a small but pos-

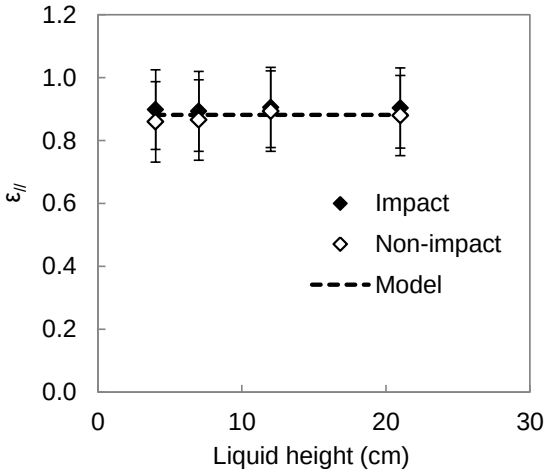

Figure 15: The effect on effectiveness of bubble-on-coil impact and liquid height for 6 mm orifices

itive effect on effectiveness which is more pronounced at low column heights. Due to the possibility of experimental error, the difference may or may not be meaningful. However, the correlation from Akita and Yoshida [13] does suggest that the initial bubble diameter is strongly correlated with the orifice diameter, and it would not be surprising if the gas-side resistance of a bubble swarm in a short column increases with increasing bubble diameter. However, no decrease in effectiveness with decreasing column depth was noticed for the bubbles which impacted the coil. In the impact case, the coil may cause the large bubbles to slow down, squish or split, all of which would reduce the resistance to heat and mass transfer to the bubble surface, giving the effect of a deeper column.

The slight difference in effectiveness between the small and large sparger orifices (Figures 12 and 15, respectively) is expected given that the case

shown in Figure 12 had a higher air inlet temperature and flow rate, both of which are shown in Figures 14 and 11 to cause lower effectiveness.

Other effects of bubble-on-coil impact such as changes in the outer coil heat transfer coefficient may also explain why in all cases a slightly higher effectiveness is observed when impact occurs. Because bubble-on-coil impact seems to cause some improvement, no matter how small, it is worthwhile to consider sparger designs that facilitate impact so long as they do not raise the system cost. This is especially true because other design choices which increase the effectiveness tend to increase the capital cost (e.g. raising the coil area) or energy use (e.g. using a narrower tube, which increases pumping power), whereas the arrangement of holes on a sparger plate is unlikley to be linked to a significant variation in cost.

4.5. Air Gap Heat Transfer

Because the vertical section of the cooling coils used in this experiment was not perfectly insulated, some heat transfer occurred between the outgoing air and the coils in the air gap above the column liquid. This fraction, calculated using the method described by Tow and Lienhard [15], which utilizes the measured pool temperature, is shown in Figure 16 for the same experiments plotted in Figures 6 and 7. No model curve is shown because the model neglects heat transfer in the air gap.

If the coil was not exposed in the air gap, the additional heat transfer in the air gap would be zero. However, the reduction in the total heat transfer rate would be much less than the percent shown in Figure 16. Heat transfer occurring in the incoming exposed coil section reduces the maximum amount of heat transfer that can occur in the column and reduces the heat

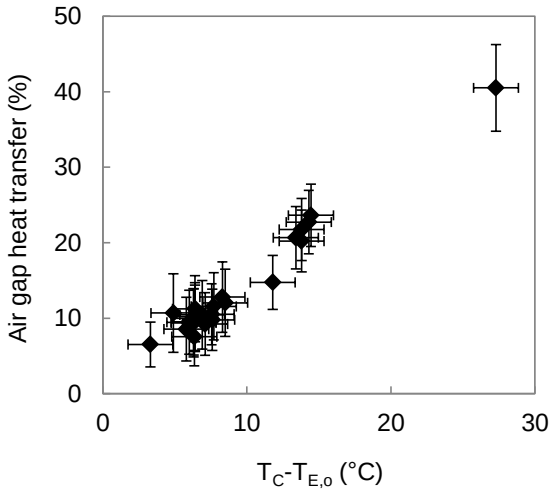

Figure 16: The percent of the total heat transfer occurring in the air gap increases with the liquid side temperature pinch, $T_C - T_{E,o}$

transfer driving force (the LMTD). If the potential for air gap heat transfer is eliminated, the maximum heat transfer rate and LMTD will rise together, resulting in a comparable effectiveness. However, the heat transfer between the outgoing air and the outgoing exposed section of coil, which occurs once both streams have completed their interaction with the column liquid, will be lost. The remaining maximum possible heat transfer rate between the outgoing air and outgoing coolant is low due to the low temperature difference between the exiting air and outgoing coolant and the low absolute humidity of the cool air. Especially because the low temperature difference also limits the heat transfer driving force, it can be concluded that the heat transfer rate is not significantly affected by the possibility of heat transfer in the air gap for reasonably high-effectiveness columns. In this experiment, there was one exception: the 8.7 cm coil section operating at low effectiveness whose

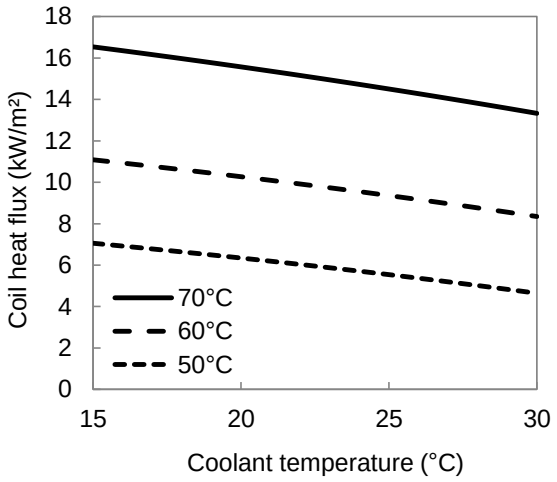

Figure 17: The heat flux decreases with increasing coolant temperature, as shown for three air temperatures

air exits the liquid at 52.0°C may transfer a significant amount of additional heat to the outgoing section of coil at a cold 24.7°C. This is consistent with the observation that the actual heat flux and effectiveness of the shortest coil were significantly higher than that predicted by the model, which neglects air gap heat transfer.

4.6. Additional Modeling Results

Given the success (quantified in Section 4.1) of the model in predicting the experimental results, it can also be used to predict the effect of additional parameters not varied in the present experiments. In this section, the effects of coolant temperature and coolant tube diameter are simulated.

Figure 17 shows that heat transfer rate decreases with increasing coolant temperature for an air flow rate is 2 L/s. A coolant temperature of 20°C is used with the same tubing and water flow rate used in the experiment. The

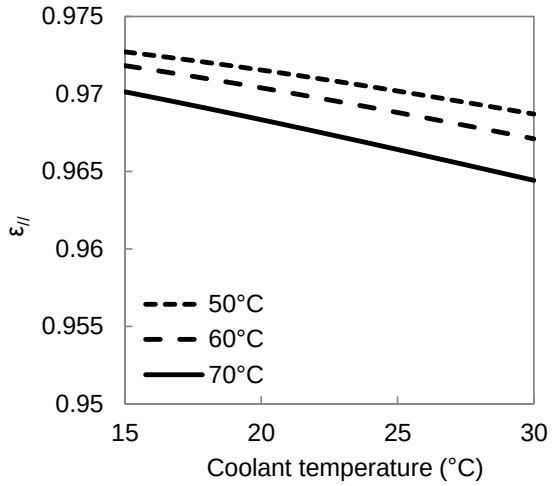

Figure 18: The effectiveness is nearly constant with changing water temperature, as shown for three air temperatures. The vertical axis is expanded to show that there is, however, a slight decrease in effectiveness with increasing coolant temperature

coil surface area is 0.05 m^2. In HDH desalination applications, the coolant temperature will often be set at the temperature of the water to be treated. However, in cases where brine is recirculated to increase water recovery and brine concentration, Figure 17 shows that the water should be cooled before recirculation to achieve the highest possible heat flux.

With changing coolant temperature, effectiveness increases with decreasing water temperature but only by less than a 1% change over the 15°C range shown. This finding contrasts with the decrease in effectiveness accompanying the increase in heat flux when air temperature is increased (see Figures 10 and 11). The difference is due to the shape of the temperature-enthalpy curve of saturated moist air. The mass fraction of water vapor in saturated cool air is low, so the heat flux increases a moderate amount as

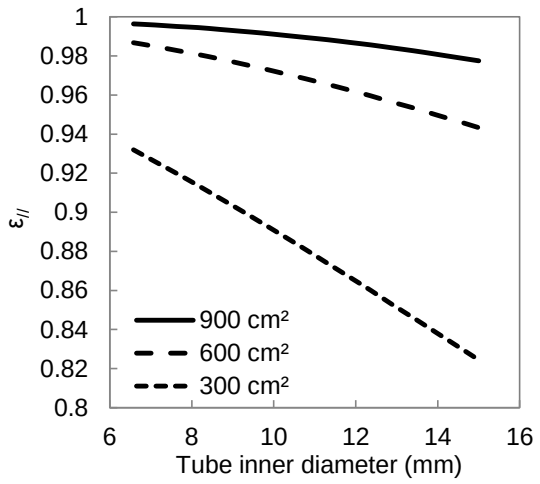

Figure 19: Decreasing the tube diameter at constant coil surface area leads to an increase in effectiveness which is more pronounced for smaller coils

the coolant temperature is decreased while the temperature driving force for heat transfer across the coil increases more strongly.

Though tube diameter was not varied experimentally, Figure 19 shows that tube diameter can significantly influence the effectiveness, especially for lower-surface-area coils. The water flow rate simulated was the same as in the experiment, the air flow rate was 2 L/s, and the air and coolant temperatures were 60°C and 20°C, respectively. Because the tube diameter is linked to the pressure drop, determining the optimal tube diameter for dehumidification in HDH desalination will require an analysis of a complete system.

5. Conclusions

A simple and accurate model predicting bubble column dehumidifier performance was presented and verified with experimental results. Due to the

large volumetric interfacial area in a bubble column, the gas-side resistance is found to be sufficiently low that it can be neglected in modeling for columns deeper than 4 cm in the homogeneous flow regime. Care should be taken to minimize column height in order to reduce the gas-side pressure drop across the dehumidifier. As is common for heat exchangers, a tradeoff exists between heat flux and effectiveness (performance parameters representing capital and energy costs) when sizing the coil. However, it is shown that high parallel-flow effectiveness can still be achieved with much smaller coils than those used in previous work. The model developed herein can be used to predict the performance of each stage of a multistage dehumidifier for the design and optimization of HDH desalination systems.

6. Acknowledgement

We would like to acknowledge support from the King Fahd University of Petroleum and Minerals through the Center for Clean Water and Clean Energy at MIT and KFUPM (Project #R4-CW-08). The first author would also like to gratefully acknowledge support from the Flowers Family Fellowship and the Pappalardo Fellowship, and thank Steven Lam for building the experimental apparatus. This material is based upon work supported by the National Science Foundation Graduate Research Fellowship Program under Grant No. 1122374.

References

[1] H. Ettouney, Design and analysis of humidification dehumidification desalination process, Desalination 183 (2005) 341 – 352.

[2] M. A. Sievers, J. H. Lienhard V, Design of flat-plate dehumidifiers for humidification dehumidification desalination systems, Heat Transfer Engineering 34 (2013) 543–561.

[3] M. A. Sievers, J. H. Lienhard V, Design of plate-fin tube dehumidifiers for humidification-dehumidification desalination systems, Heat Transfer Engineering (Accepted 2014).

[4] G. P. Narayan, M. H. Sharqawy, J. H. Lienhard V, S. M. Zubair, Thermodynamic analysis of humidification dehumidification desalination cycles, Desalination and Water Treatment 16 (2010) 339–353.

[5] G. P. Narayan, M. H. Sharqawy, S. Lam, S. K. Das, J. H. Lienhard V, Bubble columns for condensation at high concentrations of noncondensable gas: Heat-transfer model and experiments, AIChE Journal 59 (2013) 1780–1790.

[6] G. P. Narayan, J. H. Lienhard V, Thermal design of humidification dehumidification systems for affordable small-scale desalination, IDA Journal 4 (2012) 24–34.

[7] K. M. Chehayeb, G. P. Narayan, S. M. Zubair, J. H. Lienhard V, Use of multiple extractions and injections to thermodynamically balance the humidification dehumidification desalination system, International Journal of Heat and Mass Transfer 68 (2014) 422–434.

[8] G. P. Narayan, M. S. St. John, S. M. Zubair, J. H. Lienhard V, Thermal design of the humidification dehumidification desalination system:

an experimental investigation, International Journal of Heat and Mass Transfer 58 (2013) 740–748.

[9] E. C. Barrett, S. G. Dunn, Design of direct contact humidifiers and dehumidifiers using tray columns, Industrial & Engineering Chemistry Process Design and Development 13 (1974) 353–358.

[10] N. Kantarci, F. Borak, K. O. Ulgen, Review: Bubble column reactors, Process Biochemistry 40 (2005) 2263–2283.

[11] I. Leibson, E. Holcomb, A. G. Cacoso, J. J. Jacmic, Rate of flow and mechanics of bubble formation from single submerged orifices II: Mechanics of bubble formation, AIChE Journal 2 (1956) 300–306.

[12] J. Joshi, Y. Shah, Invited review: Hydrodynamic and mixing models for bubble column reactors, Chemical Engineering Communications 11 (1981) 165–199.

[13] K. Akita, F. Yoshida, Bubble size, interfacial area, and liquid-phase mass transfer coefficient in bubble columns, Industrial & Engineering Chemistry Process Design and Development 13 (1974) 84–91.

[14] E. W. Tow, J. H. Lienhard V, Analytical modeling of a bubble column dehumidifier, in: Proceedings of the ASME Summer Heat Transfer Conference, Minneapolis, MN, July 14-19, 2013.

[15] E. W. Tow, J. H. Lienhard V, Heat flux and effectiveness in bubble column dehumidifiers for HDH desalination, in: Proceedings of the International Desalination Association World Congress on Desalination and Water Reuse, Tianjin, China, Oct 20-25, 2013.

[16] W. K. Lewis, The evaporation of a liquid into a gas, Mechanical Engineering 44 (1922) 445–446.

[17] J. C. Kloppers, D. G. Kroger, The Lewis factor and its influence on the performance prediction of wet-cooling towers, International Journal of Thermal Sciences 44 (2005) 879 – 884.

[18] M. Daous, A. Al-Zahrani, A simple approach to measuring the gas phase heat and mass transfer coefficients in a bubble column, Chemical Engineering & Technology 29 (2006) 1438–1443.

[19] A. Kumar, T. E. Degaleesan, G. S. Laddha, H. E. Hoelscher, Bubble swarm characteristics in bubble columns, The Canadian Journal of Chemical Engineering 54 (1976) 503–508.

[20] Y. T. Kang, A. Akisawa, T. Kashiwagi, Analytical investigation of two different absorption modes: falling film and bubble types, International Journal of Refrigeration 23 (2000) 430–443.

[21] R. Clift, J. R. Grace, M. E. Weber, Bubbles, Drops, and Particles, Academic Press, 1978.

[22] S. Klein, Engineering Equation Solver, F-Chart Software, LLC (1992).

[23] S. Saxena, R. Vadivel, A. Saxena, Gas holdup and heat transfer from immersed surfaces in two- and three-phase bubble columns, Chemical Engineering Communications 85 (1989) 63–83.

[24] S. Kara, B. G. Kelkar, Y. T. Shah, N. L. Carr, Hydrodynamics and

axial mixing in a three-phase bubble column, Industrial & Engineering Chemistry Process Design and Development 21 (1982) 584–594.

[25] Y. Mori, W. Nakayama, Study on forced convective heat transfer in curved pipes: (1st report, laminar region), International Journal of Heat and Mass Transfer 8 (1965) 67 – 82.

[26] Y. Mori, W. Nakayama, Study of forced convective heat transfer in curved pipes (2nd report, turbulent region), International Journal of Heat and Mass Transfer 10 (1967) 37 – 59.

[27] W.-D. Deckwer, On the mechanism of heat transfer in bubble column reactors, Chemical Engineering Science 35 (1980) 1341 – 1346.

[28] S. Saxena, B. Patel, Heat transfer investigations in a bubble column with immersed probes of different diameters, International Communications in Heat and Mass Transfer 18 (1991) 467 – 478.

[29] V. Konsetov, Heat transfer during bubbling of gas through liquid, International Journal of Heat and Mass Transfer 9 (1966) 1103 – 1108.

[30] K. Muroyama, S. Okumichi, Y. Goto, Y. Yamamoto, S. Saito, Heat transfer from immersed vertical cylinders in gas-liquid and gas-liquid-solid fluidized beds, Chemical Engineering & Technology 24 (2001) 835–842.

[31] E. W. Tow, J. H. Lienhard V, Measurements of heat transfer coefficients to cylinders in shallow bubble columns, in: Proceedings of the 15th International Heat Transfer Conference, Kyoto, Japan, August 10-15, 2014 (submitted).

[32] G. P. Narayan, K. H. Mistry, M. H. Sharqawy, S. M. Zubair, J. H. Lienhard V, Energy effectiveness of simultaneous heat and mass exchange devices, Frontiers in Heat and Mass Transfer 1 (2010) 1–13.

[33] G. P. Narayan, K. M. Chehayeb, R. K. McGovern, G. P. Thiel, S. M. Zubair, J. H. Lienhard V, Thermodynamic balancing of the humidification dehumidification desalination system by mass extraction and injection, International Journal of Heat and Mass Transfer 57 (2013) 756 – 770.

[34] G. P. Narayan, Thermal design of humidification dehumidification systems for affordable and small-scale desalination, Ph.D. thesis, Massachusetts Institute of Technology, 2012.